University of Nebraska - Lincoln

DigitalCommons@University of Nebraska - Lincoln

2015

Characterization of the inflammatory phenotype of Mycobacterium avium subspecies paratuberculosis using a novel cell culture passage model

Jamie L. Everman
Oregon State University

Torsten M. Eckstein
Michigan State University, East Lansing

Jonathan Roussey
Michigan State University, East Lansing

Paul M. Coussens
Michigan State University, East Lansing

John Bannantine
USDA ARS National Animal Disease Center, john.bannantine@usda.gov

See next page for additional authors
Follow this and additional works at: https://digitalcommons.unl.edu/usdaarsfacpub

Part of the Agriculture Commons

Authors

Jamie L. Everman, Torsten M. Eckstein, Jonathan Roussey, Paul M. Coussens, John Bannantine, and Luiz E. Bermudez

Characterization of the inflammatory phenotype of *Mycobacterium avium* subspecies *paratuberculosis* using a novel cell culture passage model

Jamie L. Everman,[1,2] Torsten M. Eckstein,[3] Jonathan Roussey,[4] Paul Coussens,[4,5] John P. Bannantine[6] and Luiz E. Bermudez[1,2]

Correspondence
Luiz E. Bermudez
Luiz.bermudez@oregonstate.edu

[1]Department of Microbiology, College of Science, Oregon State University, Corvallis, OR, USA

[2]Department of Biomedical Sciences, College of Veterinary Medicine, Oregon State University, Corvallis, OR, USA

[3]Department of Microbiology, Immunology and Pathology, College of Veterinary Medicine and Biomedical Sciences, Colorado State University, Fort Collins, CO, USA

[4]Comparative Medicine and Integrative Biology Program, Michigan State University, East Lansing, MI, USA

[5]Department of Microbiology and Molecular Genetics, Michigan State University, East Lansing, MI, USA

[6]National Animal Disease Center, USDA Agricultural Research Service, Ames, IA, USA

Understanding the pathogenic mechanisms of *Mycobacterium avium* subspecies *paratuberculosis* (MAP) and the host responses to Johne's disease is complicated by the multi-faceted disease progression, late-onset host reaction and the lack of available *ex vivo* infection models. We describe a novel cell culture passage model that mimics the course of infection *in vivo*. The developed model simulates the interaction of MAP with the intestinal epithelial cells, followed by infection of macrophages and return to the intestinal epithelium. MAP internalization triggers a minimal inflammatory response. After passage through a macrophage phase, bacterial reinfection of MDBK epithelial cells, representing the late phase of intestinal mucosal infection, is associated with increased synthesis of the pro-inflammatory transcripts of IL-6, CCL5, IL-8 and IL-18, paired with decreased levels of TGFβ. Transcriptome analysis of MAP from each stage of epithelial cell infection identified increased expression of lipid biosynthesis and lipopeptide modification genes in the inflammatory phenotype of MAP. Total lipid analysis by HPLC-ES/MS indicates different lipidomic profiles between the two phenotypes and a unique set of lipids composing the inflammatory MAP phenotype. The presence of selected upregulated lipid-modification gene transcripts in samples of ileal tissue from cows diagnosed with Johne's disease supports and validates the model. By using the relatively simple cell culture passage model, we show that MAP alters its lipid composition during intracellular infection and acquires a pro-inflammatory phenotype, which likely is associated with the inflammatory phase of Johne's disease.

INTRODUCTION

Mycobacterium avium subspecies *paratuberculosis* (MAP) is the causative agent of Johne's disease, a chronic intestinal inflammatory disease that affects ruminants worldwide. The disease is particularly devastating to the dairy industry, with an economic loss estimate as high as \$1.5 billion annually in the USA alone (Ott *et al.*, 1999; Stabel, 1998). The development of new approaches for control of the disease is needed and depends on increased understanding of the pathogenesis of MAP and its interaction with the ruminant host. However, investigation of the molecular mechanisms that drive the disease is made difficult by many

factors including the long incubation period between the silent subclinical infection and the severe clinical stage of the disease, and the facilities and costs associated with housing experimentally infected animals during the development of disease. Initiation of infection occurs early in the life of a calf; however, clinical signs of disease do not appear until years after initial exposure. Infection can remain undetected for a number of years, and antigen-specific and immune signal-based diagnostic tests usually fail to identify animals in the preclinical stages of the disease. When clinical signs emerge, it is too late for therapeutic intervention, and the animal producer resorts to the culling and removal of diseased animals from the herd.

The phenotype of a bacterial population plays an important role in its ability to cause and maintain a long-term infection in the host, as it has been shown with pathogens such as *Neisseria gonorrhoeae* (Hagblom *et al.*, 1985), *Salmonella enterica* serovar Typhimurium (Diard *et al.*, 2013), *Pseudomonas aeruginosa* (Penketh *et al.*, 1983), and *Mycobacterium tuberculosis* (Ryan *et al.*, 2010). Thus, environmental and host factors may potentially influence the phenotype of MAP prior to and during infection. Early studies on this phenomenon have identified a variety of phenotypes between geographically distinct MAP isolates (Whittington *et al.*, 2011), and have illustrated proteomic differences between laboratory culture and mucosal derived isolates (Weigoldt *et al.*, 2011). MAP also develops a more invasive phenotype in response to both the hyperosmolar environment of raw milk and growth within the mammary epithelium (Patel *et al.*, 2006). As phenotypic changes are quite pervasive among pathogens and utilized to drive disease, further investigation is needed to determine if differing MAP phenotypes develop while within the host and how they affect the course of Johne's disease.

Although the study of MAP phenotypes during the disease is clearly important, there is a limited number of well-defined models used to study the interaction between MAP and the mammalian host. At present, simple *in vitro* culture models of single-cell monolayers are used to explore the interaction of MAP with the epithelial intestinal cell or with phagocytic macrophage cells. Mouse models are typically employed to investigate initiation and prevention of infection during the early stages of Johne's disease (Bannantine *et al.*, 2014; Bermudez *et al.*, 2010; Scandurra *et al.*, 2010), while goat and calf models are more commonly used to study vaccine efficacy and the later stages of the disease (David *et al.*, 2014; Facciuolo *et al.*, 2013; Hines *et al.*, 2014; Khare *et al.*, 2012). While large animals provide useful models since they are the natural ruminant hosts of MAP and progress through the entire spectrum of disease states, they come with a variety of disadvantages. Pitfalls include the necessity of large spaces, extended time-courses, and very high costs, as animal infection must be allowed to progress for many years prior to development of the clinical signs of disease. In light of the drawbacks of current models, a more elaborate *in vitro* system is needed to mimic and study the different environments encountered by MAP during infection.

Natural infection within ruminant hosts begins with the uptake of MAP by the intestinal epithelium (Bermudez & Young, 1994; Bermudez *et al.*, 2010), followed by uptake by tissue macrophages (Buergelt *et al.*, 1978; Sigurethardóttir *et al.*, 2004), and tissue dissemination likely via macrophages within the lymphatic system to sites including, but not limited to, the lymph nodes, mammary tissue, liver and epithelial tissue (Antognoli *et al.*, 2008). In this study, we describe the development of a novel *in vitro* cell culture passage model which mimics the passage of bacteria from their uptake by the intestinal epithelium, spread to the tissue phagocytes, and ultimate return to the intestinal epithelium during the later stages of infection. We demonstrate that a predominant pro-inflammatory immune response is mounted upon sequential passage of bacteria and infection of epithelial cells. Our findings led us to characterize intracellular MAP populations into non-inflammatory and inflammatory phenotypes. At the genetic level, lipid biosynthesis genes are more highly expressed in the inflammatory MAP phenotype, while lipidomic analysis shows that the inflammatory MAP phenotype has a distinct lipid profile compared to that of the non-inflammatory MAP phenotype. Using the cell culture passage model, we examined the inflammatory phenotype of MAP and tested our hypothesis that the constantly changing phenotypes of MAP may trigger the transition between the multiple disease stages during the course of infection. These bacterial changes could play a significant role in variable diagnostic results and low vaccination efficacy in populations of ruminants infected with, or at risk of, contracting MAP. Further examination of this phenomenon may provide a better platform for understanding and developing future diagnostic and treatment options.

METHODS

Bacterial preparation. *Mycobacterium avium* subspecies *paratuberculosis* strain K10 (ATCC BAA-968) was cultured at 37 °C on 7H10 agar (BD) supplemented with casein hydrolysate (1 g l^{-1}; BD), 10 % (v/v) oleic acid, albumin, glucose and catalase (OADC; Hardy Diagnostics), and ferric mycobactin J (2 mg l^{-1}; Allied Monitor) for 3–4 weeks. Prior to experiments, a bacterial suspension was made in Hanks' balanced salts solution (HBSS; Corning), passed through a 22-gauge needle to disperse clumps and allowed to settle for 10 min. The top half of the inoculum was used as a single-cell suspension for experiments as described previously (Patel *et al.*, 2006).

Mammalian cell culture. Madin–Darby bovine kidney (MDBK) epithelial cells (CCL-22) and RAW 264.7 macrophage cultures (TIB-71) were obtained from the American Type Culture Collection (ATCC). Both cells lines were cultivated in Dulbecco's Modified Eagle's Medium (DMEM) supplemented with 10 % heat-inactivated FBS (Gemini Bio-Products), at 37 °C in 5 % CO$_2$.

***In vitro* cell culture passage model.** Cell cultivation and infection schedule was completed as described (Fig. 1). MDBK cells were seeded in T-75 tissue culture flasks and grown to 80 % confluence. MAP was
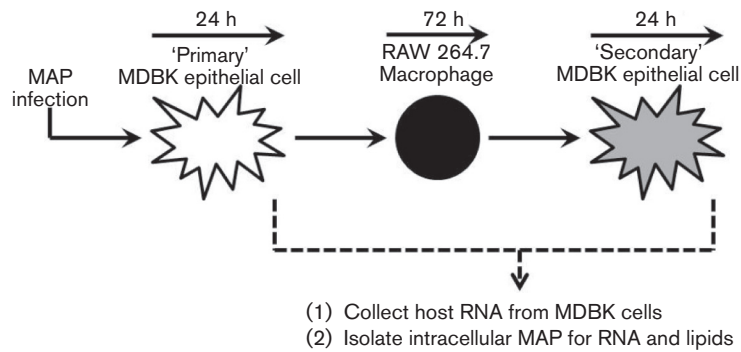
Fig. 1. *In vitro* cell culture passage model. A schematic of the cell culture passages used to mimic the path MAP takes during infection in ruminants. The time points analysed are indicated above, and samples collected for analysis of host−microbe interactions during cell culture passage are shown below.

prepared as described above and used to infect monolayers at an m.o.i. of 50 : 1 for 4 h, at which time medium was removed, cells were washed two times with HBSS and replaced in fresh medium. MAP infection proceeded for 24 h, at which time modified differential centrifugation was used to isolate bacterium from host cells as described (McNamara *et al.*, 2012). Cells were lysed with 0.1 % Triton X-100 for 15 min and lysate was centrifuged for 15 min at 2000 *g* at 4 °C. The pellet was suspended in 0.1 % Triton X-100 and centrifuged for 3 min at 60 *g* at 4 °C to remove intact cells and cell debris. The MAP-containing supernatant was collected and bacterium pelleted at 2000 *g* at 4 °C for 10 min. The bacterial pellet was suspended in HBSS, centrifuged again at 60 *g* at 4 °C to pellet any residual cell debris and MAP-containing supernatant was collected and centrifuged at 5600 *g* at 4 °C to pellet intracellular bacterium. The MAP pellet (primary MAP population) was suspended in HBSS; any bacterial clumps were disrupted by passage through a 22-gauge needle as described above and used to infect RAW 264.7 macrophages. Infection was allowed to proceed for 72 h. Macrophages were lysed and processed using differential centrifugation as described above to isolate intracellular bacterium. Single-cell suspensions were used to infect MDBK cells for 24 h, at which time differential centrifugation was used to isolate the intracellular bacterium (secondary MAP population). Mock infection passages were completed using HBSS in the absence of bacterium to account for presence of host material after differential centrifugation. MAP and mock primary and secondary populations were frozen at −80 °C for downstream analysis.

Mammalian RNA extraction and analysis. After progression through the passage model described above (Fig. 1), RNA from MDBK epithelial cells was extracted. DNase treatment was conducted using an RNeasy Mini kit as per manufacturer's instructions (Qiagen). RNA samples were verified for absence of DNA, quality verified and quantified. cDNA was synthesized using an iScript reverse transcription supermix for real-time qPCR (RT-PCR) (Bio-Rad) and transcripts were analysed using a CFX Connect Real-Time PCR Detection System (Bio-Rad) using primers listed in Table 1. PCR amplifications were run as follows: 95 °C for 3 min, 35 cycles of 95 °C for 30 s, 53 °C or 60 °C for 30 s (see Table 1 for anneal temperatures) and 72 °C for 20 s, followed by a final extension at 72 °C for 5 min, and a melt curve from 50 to 95 °C to confirm amplicon size. Relative change in gene expression was quantified using the $\Delta\Delta C_t$ method (Livak & Schmittgen, 2001). β-Actin was used as an internal normalization control for the amount of mammalian cDNA added to each reaction, and mock infection samples served as a baseline control for the immune signal profile of host cells that undergo the passage model in the absence of bacterium.

Intracellular bacterial RNA extraction. The cell culture passage model was conducted (Fig. 1) and total intracellular bacterial RNA was isolated as described (Wren & Dorrell, 2002). Briefly, infected monolayers were lysed with guanidine thiocyanate (GTC) buffer (4 M guanidine thiocyanate, 0.5 % *N*-lauryl sarcosine, 30 mM sodium citrate, pH 7.0) with 0.1 M β-mercaptoethanol, and lysates were pelleted at 2700 *g* at 4 °C. The pellet was washed twice with GTC buffer and pelleted at 2700 *g* at 4 °C. The intact bacterial pellet was lysed in Trizol (Life Technologies) with 0.5 ml of 0.1 mm glass beads by bead beating in a reciprocal bead beater for 20 s each, incubated on ice for 1 min and repeated three times. Chloroform : isoamyl alcohol (24 : 1; Ambion) was added and the mixture was centrifuged at 9500 *g* at 4 °C. The aqueous layer was collected, an equal volume of chloroform added, mixed and centrifuged at 9500 *g* at 4 °C. The aqueous layer was collected and nucleic acids were precipitated with 0.7 volume 2-propanol and 15 µg of linear polyacrylamide overnight at −20 °C. Nucleic acids were pelleted at 9500 *g* at 4 °C for 30 min, washed with 70 % ethanol and suspended in nuclease-free water. DNase treatment and RNA clean-up were performed using an RNeasy Mini kit (Qiagen) as per manufacturer's instructions. RNA preparation was verified for absence of DNA contamination and quantified. For each sample, 100 ng of RNA was amplified using a Message AmpII-Bacteria RNA Amplification kit (Ambion) as per manufacturer's instructions. Amplified RNA was synthesized using biotin-labelled UTP nucleotides (Ambion) and analysed for quality on an Agilent Bioanalyser 2100 at the Center for Genome Research and Biocomputing at Oregon State University. Samples were aliquoted and stored at −80 °C prior to microarray analysis.

Bovine CCL5 ELISA. The cell culture passage model was conducted as described above. Supernatants from the primary and secondary sets of MAP and mock-infected MDBK epithelial cells were collected after 36 h of infection. For control samples MDBK cells were infected with DMEM alone or lipopolysaccharide from *Escherichia coli* 0111 : B4 (100 ng ml^{-1}; Sigma-Aldrich) and supernatants collected. Samples were filtered through a 0.2 µm filter and used to measure the secreted chemokine CCL5 during infection using a Bovine RANTES ELISA kit (NeoBioLab) as per manufacturer's instructions.

DNA microarray. The MAP K10-specific DNA oligo spotted arrays were designed and printed at the National Animal Disease Center (USDA-ARS, Ames, IA). Arrays were post-processed, blocked and hybridized prior to use as per standard protocol (http://derisilab.ucsf. edu/microarray/protocols.html). For hybridization, total RNA was fragmented to 200 bp fragments by incubation for 30 min at 94 °C in

Table 1. Primer sets for bovine and bacterial transcript analysis

Primer	Sequence (5′–3′)	Anneal temp. (°C)	Source
Bovine			
β-Actin_B_Fwd	CGCACCACTGGCATTGTCAT	60	Konnai *et al.* (2003)
β-Actin_B_Rev	TCCAAGGCGACGTAGCAGAG	60	Konnai *et al.* (2003)
IL-6_B_Fwd	TCCAGAACGAGTATGAGG	53	Konnai *et al.* (2003)
IL-6_B_Rev	CATCCGAATAGCTCTCAG	53	Konnai *et al.* (2003)
IL-8_B_Fwd	TGCCTCATGTACTGTGTGGG	60	Weiss *et al.* (2002)
IL-8_B_Rev	GGGATAAAGAAACCAAGGCG	60	Weiss *et al.* (2002)
TGF-β_B_Fwd	TTCTTACCCTCGGAAAATGCCATCC	60	This paper
TGF-β_B_Rev	CCATCAATACCTGCAAAGCGTG	60	This paper
CCL5_B_Fwd	CATGGCAGCAGTTGTCTTTATCA	53	This paper
CCL5_B_Rev	CTCTCGCACCCACTTCTTCTCT	53	This paper
IL-18_B_Fwd	TCTTTGAGGATATGCCTGATTCTG	60	This paper
IL-18_B_Rev	CAGACCTCTAGTGAGGCTGTCCTT	60	This paper
MAP			
MAP_16s_Fwd	CGAACGGGTGAGTAACACG	60	This paper
MAP_16s_Rev	TGCACACAGGCCACAAGGGA	60	This paper
IS900_Fwd_C	GATGGCCGAAGGAGATTG	60	This paper
IS900_Rev_C	CACAACCACCTCCGTAACC	60	This paper
MAP2131_Fwd	CGTCGATGGTCAGGGCCGA	60	This paper
MAP3121_Rev	AGCAGATTCGGATGTCGGCGG	60	This paper
MAP3433_Fwd	CCCGAAGTCGACGAGGCGTT	60	This paper
MAP3433_Rev	TGCCGACCTGCAGCCAGAAG	60	This paper
MAP2974c_Fwd	GGCGTGGGAACCACCAAAAGTG	60	This paper
MAP2974c_Rev	GATCTGCGGGTGCACGACCTG	60	This paper
MAP1584c_Fwd	GGCGATCTTGTCGCTGACCTCG	60	This paper
MAP1584c_Rev	TCAACCGGCTGACCGACCCG	60	This paper

fragmentation buffer (100 mM potassium acetate, 30 mM magnesium acetate and 40 mM Tris-acetate). Array chips were hybridized with 6 µg of biotinylated RNA for 16 h using an InSlide Hybridization Oven (Thomas Scientific) in a humidified chamber at 45 °C. Chips were washed for 5 min in 5 × Saline-Sodium Citrate SSC/0.01 % SDS buffer, 3 min in 0.5 × SSC buffer and 30 s in 0.1 × SSC buffer, stained with streptavidin-Cy3 (Life Technologies) in 10 % BSA in HBSS for 1 h, and washed again in 5 × SSC/0.01 % SDS buffer for 5 min, 0.5 × SSC for 1 min and 0.01 × SSC for 10 s, and slides were centrifuged to dry. Array chip fluorescence was measured using the Axon4000 slide reader at the Center for Genome Resources and Bioinformatics at Oregon State University. Hybridization fluorescence was analysed using Axon4000 software and spots containing bubbles, scratches or inconsistency in fluorescence across the circle were censored from the data. Triplicate spots on each array were averaged and each slide was normalized to control spots containing hybridization buffer only. Triplicate biological replicates were averaged (median) and the ratio of the fluorescence values of secondary MAP/primary MAP was determined. Fluorescence values were normalized to hybridization buffer spots within each individual array chip. To confirm microarray data, cDNA was synthesized from bacterial RNA using iScript reverse transcription supermix for RT-qPCR (Bio-Rad) and each sample was run in triplicate for each time point analysed. Primers were designed for 100–200 bp amplicons with one primer located within the 70 bp oligomer spotted onto the microarray chip (Table 1). PCR amplifications were run as follows: 1 µl cDNA, 0.2 µM forward primer, 0.2 µM reverse primer, 12.5 µl SsoAdvance SYBR Green Supermix (Bio-Rad) and water to 25 µl. PCR conditions were 95 °C for 3 min, 35 cycles of 95 °C for 30 s, 60 °C for 30 s, 72 °C for 20 s, followed by a

final extension at 72 °C for 5 min and a melting curve from 50 °C to 105 °C to confirm amplicon size.

The data discussed in this publication have been deposited in NCBI's Gene Expression Omnibus (Edgar *et al.*, 2002) and are accessible through GEO Series accession number GSE62566 (http://www.ncbi.nlm.nih.gov/geo/query/acc.cgi?acc=GSE62566).

Lipid analysis of intracellular bacterial phenotypes. Intracellular bacterial samples isolated from the *in vitro* cell culture model were collected and stored at −80 °C. Samples were lyophilized and whole cell lipids were extracted by chloroform : methanol (2 : 1), dried under nitrogen, and purified using Folsch wash (chloroform : methanol : water, 4 : 2 : 1) (Eckstein *et al.*, 2006). Isolated lipids were separated by HPLC fractionation and analysed in both positive and negative mode by ES-MS as previously described (Sartain *et al.*, 2011) at the Central Instrument Facility at Colorado State University. Total spectrum of lipid ions of 200 to 3000 *m/z* are reported and phenotype-specific peaks were determined by the subtraction of the ion abundance of each phenotype from the other.

MAP-infected bovine ileal tissue. MAP-infected intestinal tissue was obtained from cattle involved in a previously approved study at Michigan State University. From dissected ileal tissue, 1 cm³ biopsy samples were collected, washed twice in PBS, snap frozen in liquid nitrogen and stored at −80 °C. Specimens were thawed in RNAlater-ICE tissue transition solution (Life Technologies) as per manufacturer's instructions. Tissue (200 mg) was dissected from each sample and homogenized in GTC buffer with 3.2 mm stainless steel beads for 2 min at setting 8 in a Bullet Blender (Next Advance). The

homogenate was transferred to a new tube and intact bacterium and debris pelleted at 5500 **g** for 5 min at 4 °C. The pellet, containing bovine tissue debris and MAP, was collected in GTC buffer and intracellular bacterial RNA was purified as described above. For complete removal of genomic DNA, samples first underwent DNase treatment and RNA clean-up (Qiagen), then were processed with a second DNase treatment with 20 U RNase-free DNase (Roche), and 20 U RNase-OUT (Life Technologies) for 20 min, followed by RNA clean-up (Qiagen). Samples were tested for presence or absence of DNA by PCR for bovine β-actin using primers listed in Table 1 and were amplified as follows: 95 °C for 30 s, 60 °C for 30 s, 68 °C for 30 s and repeated for 40 cycles. Bacterial RNA was enriched using a MICROBEnrich kit (Ambion) as per manufacturer's instructions. cDNA was prepared using an iScript cDNA Synthesis kit (Bio-Rad) and used as DNA template for PCR detection of bacterial transcripts. PCR amplification reactions were conducted using the primer sets in Table 1 and amplification proceeded as described above. Amplicons were resolved on a 1 % agarose gel and band intensities analysed using ImageJ software (Schneider et al., 2012).

Statistical analysis and data interpretation. Results are reported as the mean of three repeated experiments ± SD. Statistical comparisons between experimental groups and control groups were determined using the Student's t-test with $P < 0.05$ denoting statistical significance. GraphPad Prism version 6.0 software was used for the construction of graphs, data interpretation, and statistical analysis.

RESULTS

Development of a novel *in vitro* cell culture passage model

To readily understand the progression of MAP pathogenesis, we developed an *in vitro* cell culture passage model that mimics the interactions between the bacterium and the host intestine over the course of infection. The goal of this study was to investigate the bacterial and cellular mechanisms and their changes over the course of infection, specifically focusing on the changes that occur within the epithelial cells between the early and late stages of infection. Our illustrated model (Fig. 1) consists of consecutive passages of MAP through host cells starting with MDBK epithelial cells, continuing with dissemination into macrophages, and the final return to the intestinal epithelium. MDBK epithelial cells serve as an excellent model of the intestinal barrier and have been used to study the pathogenesis of many other pathogens. The cellular progression design of the model simplifies and replicates the stages that MAP goes through during infection of the host. Upon oral uptake of MAP from either the environment or faecal-contaminated food and water, MAP first interacts with and invades the intestinal epithelium (Bermudez et al., 2010). After translocation through the epithelial cells, bacterium are ingested by local and infiltrating macrophages in response to infection, where MAP is able to reside and replicate. Following macrophage infection, we hypothesize that during the late stage of infection bacterium are released by macrophages, during either granuloma formation, cell-mediated death or bacterial-mediated escape to encourage spread of the disease. This release would result in the subsequent return to, and infection of, the

intestinal epithelium during the late stage of the disease, and is supported by *in vivo* evidence that MAP can be identified within the intestinal epithelium during the late stage of Johne's disease in ruminants (Antognoli et al., 2008; Khan et al., 2010). Time points were determined based on the relative progression of the disease in the host. Invasion and translocation through the intestinal epithelium occurs within a short amount of time following infection, and thus we determined 24 h infection of each epithelial infection stage would be effective in modelling the infection. Furthermore, intracellular infection in macrophages can persist for long amounts of time, and requires the intracellular environment for efficient growth, replication and evasion of the immune response. Due to this, we chose a 72 h time point for macrophage infection as an appropriate representation of the survival and time within macrophages in our model. As our focus was on the hypothesized changes occurring between each stage of epithelial cell infection, we collected nucleic acids and lipids from the mammalian epithelial cells and the isolated bacterial samples during the completion of the model for further analysis. The development of the *in vitro* passage model described here represents a novel technique in which the intricate host–microbe interactions during various stages of infection may be analysed in a simplified manner, compared to current animal infection models for Johne's disease.

Serial passage of MAP initiates inflammatory response in bovine epithelial cells

To investigate if there is a change in the host immune response to infection with cell culture-passaged compared with non-passaged bacteria, we employed the model described in Fig. 1. Complete passages were conducted with MAP bacteria, as well as passages with HBSS to serve as a control (mock) infection to account for any carry-over of mammalian components during isolation of intracellular MAP. MDBK epithelial cell RNA was collected 24 h after each MAP or mock infection, cDNA was analysed for bovine cytokine and chemokine signals, and the expression ratios of MAP-infected MDBK epithelial cells to mock-infected MDBK cells were determined (Fig. 2a). Gene expression analysis revealed that the secondary epithelial cell population produced a gene expression profile of immune signals different from the primary infected MDBK cells in the model. An increase in transcripts of the pro-inflammatory signals IL-6 and IL-8 was seen only in the second infected MDBK cell population. This secondary MDBK cell population also showed a significant decrease in the expression of the anti-inflammatory signal TGFβ, compared to primary infected MDBK cells ($P < 0.005$). While secondary epithelial cells infected with MAP slightly increased expression of the pro-inflammatory signals IL-18 and CCL5 when compared to mock-infected cells, primary cells infected with MAP appeared to suppress the expression of CCL5 and IL-18. Together, the secondary infected MDBK cells had a significant increase in the
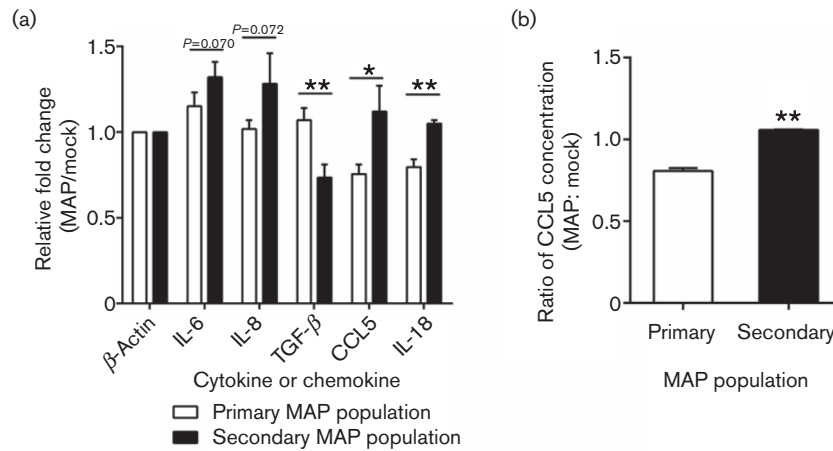
Fig. 2. Inflammatory response of MDBK epithelial cells during *in vitro* cell culture passage model. *In vitro* cell culture passage model was completed with MAP—infection and mock—infection, and RNA (a) or supernatants (b) were collected from the primary and secondary MDBK cell populations. (a) Relative expression of IL-6, IL-8, TGFβ, CCL5 and IL-18 was analysed by qPCR. Samples were normalized to β-actin expression in each sample and the relative fold changes of MAP-infected to mock-infected transcripts are reported. (b) Supernatants were collected after 36 h of infection of each epithelial cell population and concentration of CCL5 was measured using ELISA. Data represent the mean ± SD of two independent experiments analysed by qPCR or ELISA in duplicate (*P-value <0.05, **P-value <0.005 by Student's *t*-test).

transcript presence of CCL5 ($P<0.05$) and IL-18 ($P<0.005$) compared to MAP-infected primary population of MDBK cells in our model. To confirm our findings, ELISA was performed to detect the secreted CCL5 protein in the supernatants of MAP-infected MDBK cells from the passage model (Fig. 2b). Supernatant samples collected from the secondary MAP-infected epithelial cells demonstrated a higher level of CCL5 protein production and secretion than the measured expression level of CCL5 from the primary set of infected MDBK epithelial cells. Collectively, our results indicate that early infection with unpassaged MAP in the primary MDBK epithelial population induces a decreased inflammatory state within epithelial cells. Conversely, the secondary MDBK epithelial cell population infected with cell culture-passaged MAP exhibits a more inflammatory profile by means of increased pro-inflammatory (IL-6, IL-8, IL-18 and CCL5) cytokine and chemokine expression and by decreased anti-inflammatory (TGFβ) signals detected. These data suggest that during passage through host cells, MAP likely develops a novel phenotype responsible for the induction of a more pro-inflammatory immune response during infection with intracellular-conditioned MAP.

Bacterial gene expression changes during *in vitro* passage model

To determine the bacterial phenotype change during the cell culture passage model, we profiled MAP gene expression at each stage of MDBK epithelial cell infection. Intracellular MAP was collected from both primary and

secondary MDBK cell populations after 24 h of infection, and RNA from intracellular MAP was extracted and hybridized to MAP K10 DNA arrays for transcriptome analysis. Genome-wide expression analysis was completed by comparing the phenotype of MAP isolated from the secondary epithelial host cells to MAP isolated from the primary set of MDBK cells (Table 2). Our analysis identified 52 genes upregulated more than twofold in the inflammatory phenotype of MAP, when compared to the non-inflammatory primary phenotype. The upregulated genes could be categorized into three general categories: lipid biosynthesis and metabolism (MAP2974c, MAP3121 and MAP3763c), cell wall remodelling (MAP1584c, MAP0385, MAP2604c and MAP1137c) and cellular metabolism (MAP2660, MAP0808 and MAP1485c). A regulator of the transcription factor Sig8 (MAP3111c) was upregulated, as well as a variety of hypothetical proteins that have yet to be fully described (MAP3433 and MAP3516). Our results confirm the original hypothesis that intracellular passage of MAP through host cells elicits a change in gene expression, particularly in genes involved in lipid and cell wall components of the bacteria.

Lipidomic changes in MAP during passage model infection

Gene expression studies uncover substantial information on the transcriptional state of an organism. The production of macromolecules including lipids can require a variety of genetic components, non-ribosomal peptide synthase enzymes and post-translational modifications prior to

Table 2. Microarray analysis of MAP phenotypes

Intracellular MAP was isolated after 24 h from each MDBK cell population during infection using the *in vitro* cell culture passage model. Extracted bacterial RNA was amplified to biotinylated amplified RNA, and hybridization to a MAP K-10 microarray slide was measured using a streptavidin-Cy3 probe on an Axon4000 slide reader. Data represent the mean value of three independent experiments with gene oligomers spotted in triplicate on each slide and are reported as the ratio of gene expression of MAP from the secondary MDBK population to gene expression of MAP from the primary MDBK population.

Gene	Fold change	Gene description	Biological process
MAP2974c	3.20	Cyclopropane-fatty-acyl-phospholipid synthase 1	Lipid biosynthesis
MAP3121	3.14	Enoyl-CoA hydratase	Lipid metabolism
MAP3433	2.99	Hypothetical protein	Unknown
MAP3763c	2.98	Conserved polyketide synthase-associated protein 3	Lipid metabolism
MAP1584c	2.92	ATP-dependent Lon protease	Stress response proteolysis
MAP2660	2.85	NAD-dependent epimerase dehydratase	Nucleic acid metabolism
MAP0385	2.82	Restriction endonuclease family protein	DNA binding
MAP0808	2.81	Molybdenum cofactor biosynthesis protein	Metabolism
MAP3111c	2.81	Regulator of Sig8	Metabolism
MAP3516	2.77	Hypothetical protein	Unknown
MAP1456	2.76	Hypothetical esterase lipase	Metabolism
MAP1485c	2.72	Acyl-CoA synthase	Metabolism
MAA2452	2.72	Hypothetical protein	Unknown
MAP1137c	2.71	Aminoglycoside tetracycline-transport membrane protein	Membrane transport
MAP0350	2.70	Short chain dehydrogenase	Oxidoreductase
MAP2604c	2.68	Mycocerosic acid synthase	Oxidoreductase
MAP2239	2.67	Mmpl4 protein	Unknown
MAP2751	2.67	21 kDa protein	Unknown

production of a functional moiety. This can result in a skewed ratio of gene expression transcripts to translated functional lipid or protein components. As lipids play a pivotal role in mycobacterial pathogenesis, we analysed the total lipid composition of both MAP phenotypes before and after serial passage through host cells in order to ascertain the changes in the bacterial lipidome. Intracellular MAP was collected after 24 h of infection from both the primary and secondary MDBK cell populations and whole cell lipids were extracted and analysed using HPLC-ES/MS (Fig. 3). The complete lipidome spectrum between the primary passaged MAP population (Fig. 3a) and secondary passaged inflammatory MAP population (Fig. 3b) have similarities in the composition of common small ion fragments from 200 to 300 *m/z*, and in mycolic acid ion patterns found from 1000 to 1500 *m/z*. Conversely, there are dramatic differences in the lipid profiles detected from 300 to 900 *m/z* between the MAP phenotype isolated from the primary epithelial cell infection (Fig. 3c) and the inflammatory MAP phenotype isolated from the secondary epithelial cell infection (Fig. 3d). Focusing on the differences within that range, whole cell lipidome profiles were analysed for lipids specific to each population. The inflammatory phenotype of MAP is composed of a much more diverse set of lipids, including a wider array of specific sizes and types of lipids (Fig. 3f), compared to those specific to the primary MAP population (Fig. 3e).

The mycobacterial lipid Para-LP-01 has been described as an important cell wall component of MAP (Eckstein *et al.*, 2006). Para-LP-01 is known to decrease in abundance following intracellular infection (Alonso-Hearn *et al.*, 2010). We used this molecule as an internal validation marker for our model (Fig. 4). When comparing the two phenotypes, Para-LP-01 was found in high abundance in the lipidomic spectrum of the primary MAP phenotype at an intensity of 7.7×10^4 (Fig. 4a), while the lipid composition of the cell culture-passaged inflammatory phenotype contained a significantly lower abundance of Para-LP-01 at an intensity of 3.0×10^3 (Fig. 4b). The loss of Para-LP-01 and differences in other lipids in the late infection phenotype suggest that the change in lipid composition may contribute to the inflammatory status within the intestinal epithelium during MAP infection of the ruminant host.

Identification of upregulated MAP transcripts from infected tissues

In order to validate the *in vitro* cell culture passage model, we selected upregulated MAP genes from the secondary inflammatory phenotype and investigated the presence of these transcripts in the tissue samples of MAP-infected animals. Two cattle at a Michigan dairy were identified as MAP-positive by standard diagnostic techniques including faecal PCR and ELISA detection of MAP antibodies (data not shown). The high level of bacterial burden measured by qPCR, and observations of abnormal peripheral blood
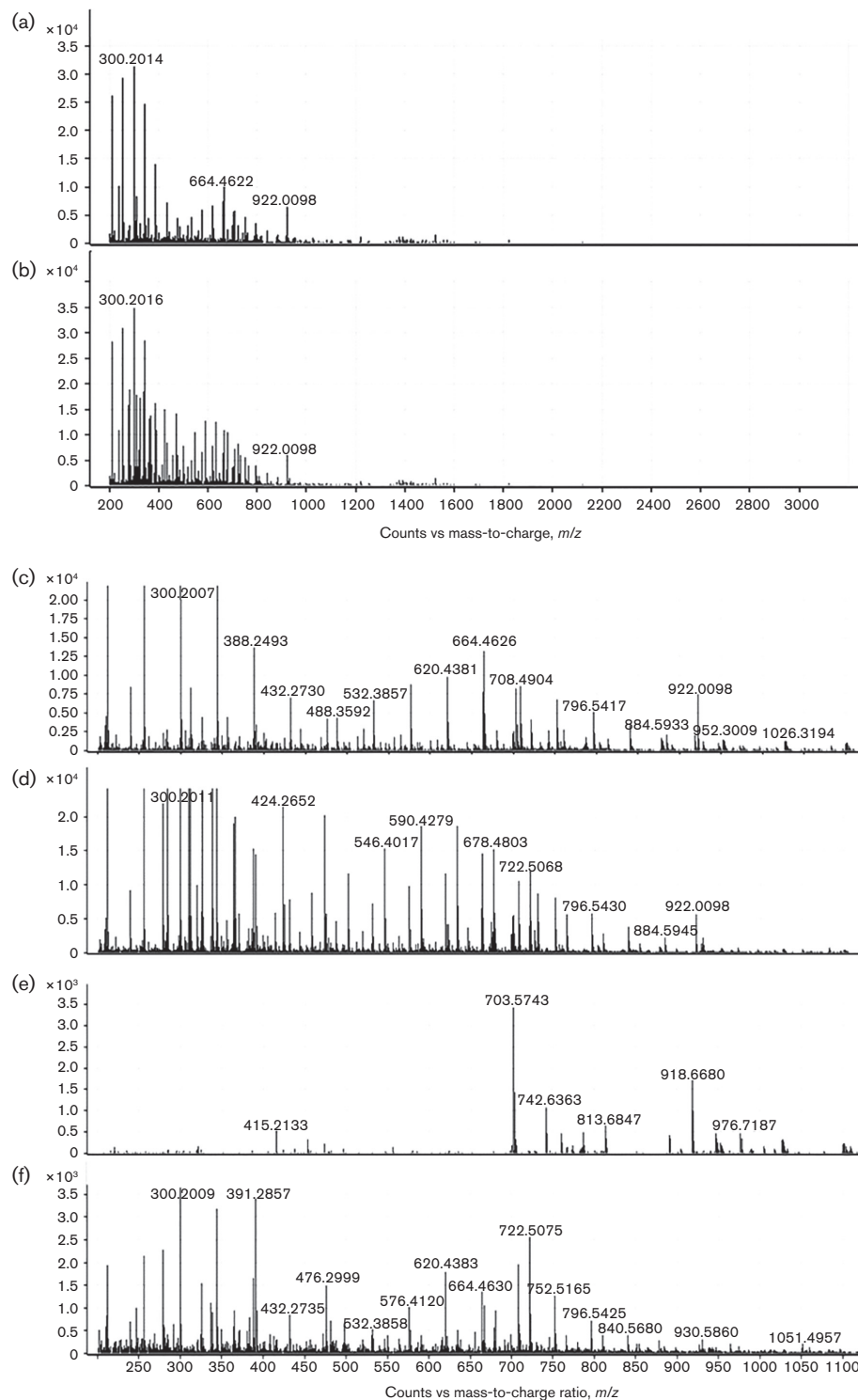
Fig. 3. Lipid profiles of MAP phenotypes. Intracellular MAP populations were isolated after 24 h of infection using the *in vitro* cell culture passage model and total lipid extraction was performed and analysed using HPLC-ES/MS. The complete spectra of 200 to 3000 *m/z* are shown (a, b) as well as a more detailed representation of the spectra from 200 to 1100 *m/z* (c, d). The lipidome of the primary population phenotype (a, c) and the secondary inflammatory phenotype (b, d) have distinct differences in both the presence and abundance of detected lipid ion fragments. Lipid ions unique to the primary population phenotype (e) and the secondary inflammatory phenotype (f) are shown. Unique lipid profiles were determined by subtracting abundance values of each lipidome from one another. The ion of 922.0098 *m/z* represents the internal standard which was added to each sample prior to analysis. Spectra in (a) and (b) are shown with the same *x*-axis range; spectra in (c–f) are shown with the same *x*-axis range.
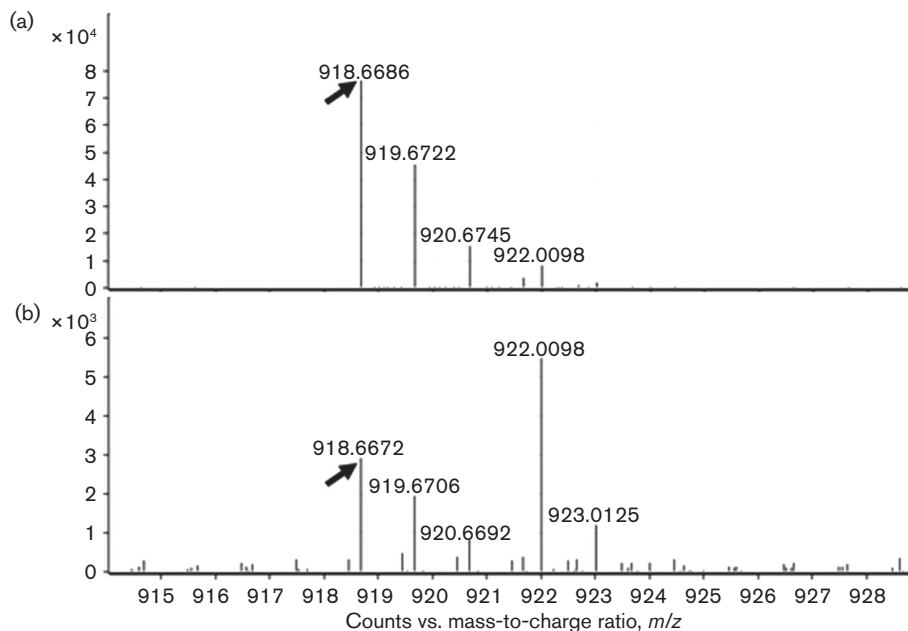
Fig. 4. Abundance of cell wall lipid Para-LP-01 in MAP phenotypes. Intracellular MAP populations were isolated after 24 h of epithelial cell infection using the *in vitro* cell culture passage model and equal amounts of total lipids were analysed using HPLC-ES/MS. The ion of size 918.66 *m/z*, known as Para-LP-01 (arrow), was identified as running in identical fractions of HPLC eluate (data not shown) with intensity of the fragment in the primary MAP population at 7.7×10^4 (a), and intensity in the inflammatory MAP phenotype at 3.0×10^3 (b). The ion of 922.0098 *m/z* represents the internal standard which was added to each sample prior to analysis. Spectra (a) and (b) are shown with the same *x*-axis range.

mononuclear cell counts indicated that one animal was in the advanced stages of Johne's disease (animal no. 6211; Fig. 5b and data not shown), while another exhibited a sub-stantially lower level of bacterial shedding, was in relatively good body condition and had normal peripheral mono-nuclear cell counts (animal no. 1688; Fig. 5a and data not shown). Tissue samples were collected from various locations within the terminal ileum during necropsy, and total RNA was isolated and analysed for the presence of bacterial transcripts (Fig. 6a). Within each tissue sample, the MAP insertion element IS*900* was detected in abun-dance, indicating MAP infection in each particular tissue section. The presence of MAP3121, MAP3433, MAP2974 and MAP1584 transcripts was detected within at least one ileal tissue sample from each of the infected animals. It was observed that detection levels within each tissue biopsy appeared to be correlated with areas that were observed to have more significant lesions during necropsy (lesion 2 in animal no. 1688 and lesion 1 in animal no. 6211). Band intensity determined that levels of the inflam-matory phenotype-related MAP transcripts in animal no.6211 were higher than those found in animal no. 1688. Interestingly, animal no. 6211 was in a more advanced clinical stage of Johne's disease, as observations indicated the animal had stopped eating and was almost unable to stand. Necropsy and diagnostics indicated a greater degree of inflammation within the ileal tissue, and

almost 100 times more MAP was detected in faecal qPCR tests. In contrast, animal no. 1688 was visually healthy, active and mobile, and had a lower grade of inflammation observed upon gross examination of the ileal tissue (obser-vational data). The identification of inflammatory MAP phenotype transcript markers within naturally occurring MAP-infected cattle, and the increase of these markers in tissue from an animal in the much more progressive stages of Johne's disease, provide evidence that supports the validity of the findings reported using the described cell culture passage model.

DISCUSSION

The shift in the host immune response is a key character-istic to the onset of inflammation within the intestinal tissue of ruminants, and results in the distinct character-istics of Johne's disease. While cell culture and animal models have uncovered intracellular survival mechanisms, little is known about the bacterial drivers behind the tran-sition in the immune response and progression to the clini-cal stage of the disease. In this paper, we describe a novel cell culture passage model which mimics the progression of infection within the tissues of the host. Using this model, we identify two different bacterial phenotypes that trigger opposite levels of inflammatory signals produced
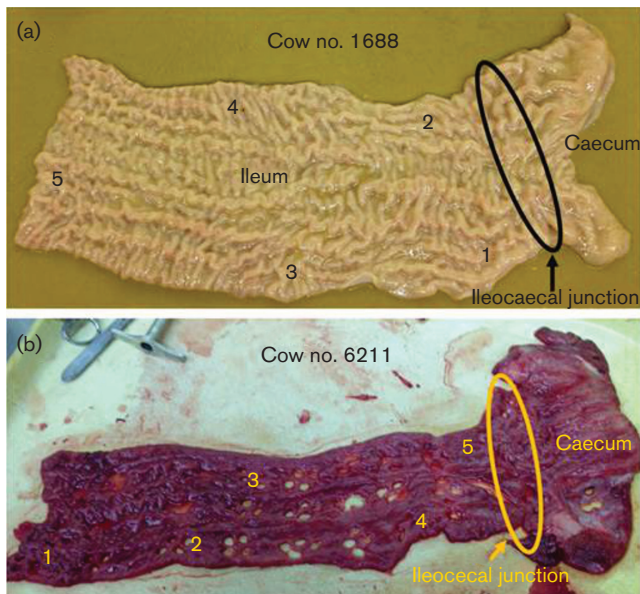
Fig. 5. Bovine intestinal tissue samples. Tissue samples from animals testing positive for Johne's disease were collected from the terminal ileum of each animal. Animal no.1688 (a) was in a much healthier state, while animal no. 6211 (b) was extremely weak, in poor body and immune condition and in a much later stage of infection. Biopsy punches were taken from locations indicated (1–5) after photograph (a), and prior to photograph (b), and immediately snap-frozen for downstream sample processing.

by infected epithelial cells, similar to the pattern of the infection in cows. These data indicate that MAP alters its phenotype during intracellular infection, and the lipid composition of the bacterium changes and we hypothesize that those changes potentially contribute to the shift in the inflammatory response by the infected host epithelial cells during Johne's disease.

Current disease models used to study Johne's disease include *in vitro* cell culture systems which provide important information on bacterial virulence mechanisms, yet the scope of infection is limited to the cellular level of a single particular cell line. Mouse models are used to investigate the ability of MAP to invade the intestinal mucosa and disseminate to peripheral tissues (Bermudez *et al.*, 2010), to determine preventive probiotics (Cooney *et al.*, 2014) and to identify and validate vaccine candidates (Bannantine *et al.*, 2014; Scandurra *et al.*, 2010). Unfortunately, mouse models offer limited insight on the complete disease progression, as mice do not exhibit intestinal inflammation in the same manner as ruminants in advanced stages of Johne's disease. MAP infections of goat and calf models are used to study a variety of disease interactions including host gene expression (Khare *et al.*, 2012), vaccine efficacy (Hines *et al.*, 2014), both bacterial (Facciuolo *et al.*, 2013) and host (David *et al.*, 2014) biomarker discovery for enhanced diagnostics, and are used to track and develop

mathematical shedding and transmission models (Mitchell *et al.*, 2008); however, the excessive time and space costs of large animals make ruminant models challenging to use. Though recent efforts have been made to standardize animal models used in Johne's disease research (Hines *et al.*, 2007), historical literature lacks consistency. A review of the past century of Johne's disease literature reveals a high level of variation in study design variables (Begg & Whittington, 2008). These inconsistencies allow past Johne's animal studies to be open to a wide array of interpretation as to how those varying factors and the particular animal host used accurately and consistently model the full stages of Johne's disease infection. With this knowledge, we aimed to develop a passage model system composed of cell lines to simulate the more complex interactions occurring within the intestinal tissue of the host (Fig. 1). By utilizing this model, we will be able to more readily understand both the host and bacterial mechanisms used during the invasion and infection process of the ruminant intestine, and discover unidentified changes or interactions that occur during the disease.

During natural infection, ruminants are infected with MAP via intestinal epithelial cell uptake and the bacterium are ingested by resident and infiltrating macrophages in the epithelial tissue. MAP-containing macrophages can then traffic throughout the host, leading to system dissemination of the bacterium as demonstrated by the detection of MAP from a variety of organs including mesenteric lymph nodes, liver, muscle tissue, mammary lymph nodes, epithelium and intestinal mucosa (Alonso-Hearn *et al.*, 2009; Antognoli *et al.*, 2008; Sweeney *et al.*, 1992). Infected macrophages located in the epithelial tissue can then lead to the formation of granulomatous lesions within the mucosa. Once a high enough intracellular burden has been reached, MAP can trigger necrosis within infected bovine macrophages (Periasamy *et al.*, 2013), suggesting that necrotic macrophages in the early stages of granuloma formation may contribute returning MAP to the host epithelium during the progression of Johne's disease. The model described here, and the inflammatory signals measured during the differing stages of infection, are supported by the scientific literature which has reported the subclinical and clinical stages of Johne's disease and analysed the immunological responses specific to the mucosal intestinal tissue during each stage (Buza *et al.*, 2003; Khare *et al.*, 2012; Lee *et al.*, 2001; Stabel & Robbe-Austerman, 2011; Weiss *et al.*, 2006). Experimental observations support the role of induced immune tolerance in mucosal tissue during early stages of Johne's disease. TGFβ is capable of inducing 'inflammatory anergy' in human macrophage cells, as they maintain phagocytic capabilities, but are unable to mount a proper pro-inflammatory cytokine response (Smythies *et al.*, 2005). Weiss *et al.* (2006) have reported that although the total T-cell population increases during MAP infection in cattle, the majority of those cells are memory ($CD2^+CD62L^-$) or regulatory ($CD4^+CD25^+$) cells, but it is unclear as to
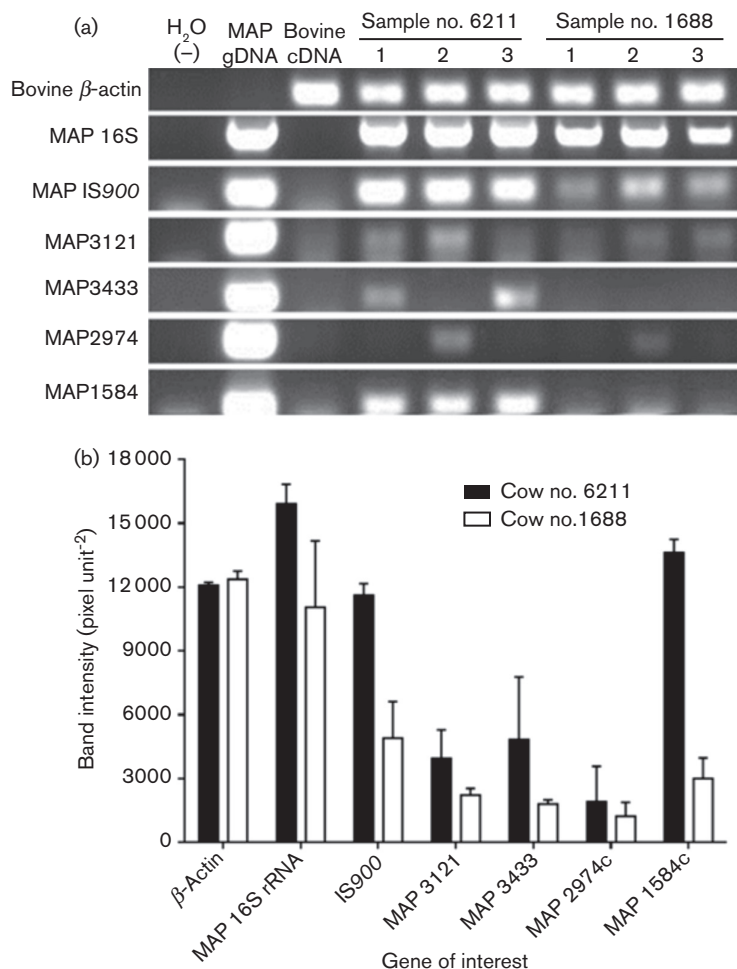
Fig. 6. MAP transcripts from infected bovine intestinal tissue. Ileal samples were collected from cattle that tested positive for MAP infection, and tissue sections were processed for RNA extraction. Bacterial–mammalian RNA sample mixtures were enriched for bacterial RNA using a MICROBEnrich kit and cDNA was used for PCR identification of inflammatory MAP phenotype transcripts (a). Gel band intensities were quantified using ImageJ and graphed (b) to show expression differences between the late-stage, severely infected animal (no. 6211; black bars) and the early stage infected animal (no. 1688; white bars). Data represents the mean measured band intensity $+/-$ SD of 3 individual tissue samples.

whether the cells deemed as regulatory T-cells in the study were under the control of FoxP3 activation. Additionally, host gene expression analysis has identified a variety of T-cell, cytokine and additional immune cell signalling factors that are either suppressed or not expressed at all during the early stages of MAP infection within ligated ileal loops of MAP-infected neonatal calves (Khare *et al.*, 2012). The early phenotype of MAP may play a role in inducing a transient anti-inflammatory environment to gain a foothold for increased infection outcomes. We show that IL-18 is downregulated within epithelial cells during early MAP phenotype expression. IL-18 is important in immunomodulation during mycobacterial infection, as IL-18-deficient mice are unable to stimulate interferon gamma (IFNγ) and develop an excess of granulomatous lesions in response to *M. tuberculosis* and *Mycobacterium bovis* BCG challenge (Sugawara *et al.*, 1999). IFNγ is a well-known immune

signal for combating mycobacterial disease, serves as a marker used to aid in diagnosing MAP infection and can be seen as early as 3 months after oral infection in cattle (Stabel & Robbe-Austerman, 2011). By creating an early anti-inflammatory environment within the epithelium, early MAP phenotypes may be used to create a microenvironment within the mucosal tissue which supports enhanced uptake, intracellular survival and spread of the bacterium.

In addition to epithelial infection, macrophages have been shown to respond differently following the contact with different pathogens. It is now accepted that either pathogens are capable of triggering an inflammatory response characterized by anti-microbial activity represented by the release of IFNγ (M1 subpopulation), or that pathogen stimulation can result in the production of IL-4, IL-13, IL-10 or TGFβ, and behave as an anti-inflammatory subpopulation, associated with Th2 stimulation and function

(Mosser & Edwards, 2008). In our study, following uptake of MAP, the phenotype of the macrophages was not investigated, although we have preliminary evidence indicating that macrophages infected with MAP produce TNFα, suggesting that the infection results in the inflammatory macrophage phenotype. Further studies will be performed to attempt to delineate if M2 macrophages develop or have any role during MAP infection.

It is well described that the alteration of the phenotype of a bacterium can be imperative to the response to and survival within a variety of environmental and host conditions. Several pathogens utilize particular phenotypes for enhanced infection, including *Neisseria meningitidis* (Hagblom *et al.*, 1985), *Staphylococcus aureus* (Tuchscherr *et al.*, 2011), and *Sal.* Typhimurium (Diard *et al.*, 2013), and a variety of mycobacterial species are reported to readily alter their phenotypes in response to external stimuli. The close relative of MAP, *M. avium* subspecies *hominissuis,* alters its phenotype upon the formation of microaggregates and biofilms (Babrak *et al.*, 2015; McNabe *et al.*, 2011), in response to the metal matrix found within host phagosomes (Early & Bermudez, 2011) and upon intracellular infection of macrophages and amoebae (Bermudez *et al.*, 2004; Harriff & Bermudez, 2009). Furthermore, previous studies with MAP indicate that changing phenotypes in response to environmental and host conditions contributes to virulence and increased pathogenesis within the host (Alonso-Hearn *et al.*, 2008; Patel *et al.*, 2006). Our data suggest that MAP changes its phenotype during the stages of intracellular infection, and that these changes involve the alteration of whole cell- and cell wall-associated lipids. These changes are pertinent, as MAP has an abundant reliance on its lipid-rich cell wall for virulence and survival (Bansal-Mutalik & Nikaido, 2014; Cambier *et al.*, 2014; Ehrt & Schnappinger, 2007). The upregulated genes we identified in this study are involved in a number of lipid-related processes. The genes MAP2974c, MAP3121, MAP3763c and MAP1584c are all involved in larger lipid synthesis gene clusters and ORFs responsible for the production of multi-domain lipid synthase enzymes required for proper lipid production. Other changes include an increase in the unique mycobacterial cell wall component mycocerosic acid (Rainwater & Kolattukudy, 1985), MAP1456 (which is located in a larger cluster of genes containing ABC-transporters) and a hypothetical transcriptional regulator encoded by MAP3111c. Interestingly, rather than being responsible for the synthesis of one specific lipid, many of the genes identified in our study seem to be specific components of the larger multi-factorial pathways required for the breakdown and biosynthesis of lipids within the bacterium. The higher expression of these genes suggests that in tandem they have the ability to more globally impact the production of lipid components. Lipid analysis conducted in this study identified ion fragment patterns of the lipidome and suggest that the change in gene expression results in an impact on total lipid composition. As seen from our data, the inflammatory phenotype of MAP is uniquely composed of a wide variety of types and sizes of lipids compared to the non-inflammatory MAP phenotype.

Changes in lipid composition, cell wall-associated molecules or the abundance of such components have the ability to dramatically impact the virulence of the bacterium prior to and during infection. One major cell wall component known to change during intracellular infection is the high molecular mass lipopeptide Para-LP-01, which is found in abundance in the cell wall of MAP and is recognized by sera from infected cattle (Eckstein *et al.*, 2006). The decrease in Para-LP-01 abundance after intracellular infection (Alonso-Hearn *et al.*, 2010) is also seen in the total lipid composition from intracellular MAP in our passage model, with significantly higher levels of Para-LP-01 present in the bacterial lipids from the bacterial population isolated from the primary MDBK cell infection. These findings provide evidence that supports the validity of the model system described in this manuscript, and that the changing lipidome may play a role in the evolving stages of Johne's disease.

The shift in mycobacterial lipid composition in response to a changing environment could result in a variety of outcomes. The immunogenic nature of mycobacterial lipids is classically demonstrated by their addition to Freund's adjuvant and its ability to elicit a robust immune response (Freund, 1956). Mycobacterial lipid components are capable of stimulating inflammatory cytokines IL-6 and TNFα when coated onto latex beads and delivered to host immune cells (Geisel *et al.*, 2005). Alternatively, this change in bacterial components could be a useful strategy in suppressing particular inflammatory responses at certain times, producing virulence factors at specific times to trigger a particular stage of the disease, and produce an environment it needs to survive. The expression levels or variation of lipoarabinomannan (LAM) and mannose-capped LAM molecules result in a change in virulence or bacterial survival as LAM is, in part, responsible for the inhibition of maturation of mycobacterium-containing phagosomes and thus contributes to intracellular survival (Fratti *et al.*, 2003). Not only does mannosylated LAM increase intracellular survival, but MAP derived molecules are capable of suppressing macrophage inflammatory signals by prolonged stimulation of IL-10 during infection (Souza *et al.*, 2013). Additional evidence demonstrates that *M. tuberculosis* utilizes its lipid moieties to modify the innate response of macrophages via TLR receptors. Differing virulence phenotypes of *M. tuberculosis* contain a different composition of lipids from one another, and infection with each strain results in opposing macrophage inflammatory phenotypes, with the most virulent strains more negatively affecting the TLR-activated cytokine response within the host phagocytes (Rocha-Ramírez *et al.*, 2008). Keeping each of these situations in mind, the variation of bacterial lipids described in this study may provide a method of camouflage for the bacterium early during infection, by interacting with TLRs and

cellular receptors and resulting in the alteration, by either suppression or stimulation, of the host immune response.

An explanation for the changing lipid phenotype during infection can also be that it is due to the energetic demands on the bacterial organism. The production of the lipids, specifically mycolic acids, which make up the majority of the cell envelope of MAP is metabolically costly. Mycocerosic acid, whose synthase (MAP2604c) is upregulated 2.68-fold in the inflammatory phenotype, is a dense lipid moiety based on a long 28- to 32-carbon backbone (Minnikin, 1982). The production of the pentapeptide component of Para-LP-01 requires a large input of energy and resources, as the gene that encodes its production is approximately 20 kb in length. The seemingly unnecessary production of such large molecules could channel required nutrients or lipid components away from pathways needed to produce functionally relevant cell wall molecules needed for the current infection stage at hand. This specifically rings true for intracellular populations which are already limited in the ions, fatty acid precursors, cholesterol and metabolic building blocks necessary for intracellular virulence and survival (Subramoni *et al.*, 2013; Tuchscherr *et al.*, 2011). Using differing phenotypes for initiation, survival and transmission ensures that the pathogen is more successful, and energetically efficient, during each particular stage of disease.

The development of the novel cell culture passage model described here enhances the ability to more readily study the intricate mechanisms occurring between the bovine host and MAP in the absence of a live animal. This model demonstrates that MAP develops an inflammatory phenotype over the course of infection, and initiates a more pro-inflammatory cytokine and chemokine response in the later stages of infection within the epithelial mucosa. The inflammatory phenotype is characterized by a distinct set of upregulated genes and contains a lipid composition distinct from the non-inflammatory phenotypes of MAP. Identification of these lipid synthesis transcripts within MAP-infected bovine tissues provides evidence which supports the validity of our model and offers evidence towards the idea that the changes in MAP, its gene expression and its lipid composition could be a driver behind the multiple stages of Johne's disease. These changes could be a notable pathogenic mechanism of interest to study, as the characterization of the function of these lipids may provide novel compounds for enhanced vaccine targets and therapeutic strategies for animals in the advanced stages of Johne's disease.

ACKNOWLEDGEMENTS

REFERENCES

Alonso-Hearn, M., Patel, D., Danelishvili, L., Meunier-Goddik, L. & Bermudez, L. E. (2008). The *Mycobacterium avium* subsp. *paratuberculosis* MAP3464 gene encodes an oxidoreductase involved in invasion of bovine epithelial cells through the activation of host cell Cdc42. *Infect Immun* **76**, 170–178.

Alonso-Hearn, M., Molina, E., Geijo, M., Vazquez, P., Sevilla, I., Garrido, J. M. & Juste, R. A. (2009). Isolation of *Mycobacterium avium* subsp. *paratuberculosis* from muscle tissue of naturally infected cattle. *Foodborne Pathog Dis* **6**, 513–518.

Alonso-Hearn, M., Eckstein, T. M., Sommer, S. & Bermudez, L. E. (2010). A *Mycobacterium avium* subsp. *paratuberculosis* LuxR regulates cell envelope and virulence. *Innate Immun* **16**, 235–247.

Antognoli, M. C., Garry, F. B., Hirst, H. L., Lombard, J. E., Dennis, M. M., Gould, D. H. & Salman, M. D. (2008). Characterization of *Mycobacterium avium* subspecies *paratuberculosis* disseminated infection in dairy cattle and its association with antemortem test results. *Vet Microbiol* **127**, 300–308.

Babrak, L., Danelishvili, L., Rose, S. J., Kornberg, T. & Bermudez, L. E. (2015). The environment of *Mycobacterium avium* subsp. *hominissuis* microaggregates induces the synthesis of small proteins associated with efficient infection of the respiratory epithelial cells. *Infect Immun* **2**, 625–636.

Bannantine, J. P., Everman, J. L., Rose, S. J., Babrak, L., Katani, R., Barletta, R. G., Talaat, A. M., Gröhn, Y. T., Chang, Y. F. & other authors (2014). Evaluation of eight live attenuated vaccine candidates for protection against challenge with virulent *Mycobacterium avium* subspecies *paratuberculosis* in mice. *Front Cell Infect Microbiol* **4**, 88.

Bansal-Mutalik, R. & Nikaido, H. (2014). Mycobacterial outer membrane is a lipid bilayer and the inner membrane is unusually rich in diacyl phosphatidylinositol dimannosides. *Proc Natl Acad Sci U S A* **111**, 4958–4963.

Begg, D. J. & Whittington, R. J. (2008). Experimental animal infection models for Johne's disease, an infectious enteropathy caused by *Mycobacterium avium* subsp. *paratuberculosis*. *Vet J* **176**, 129–145.

Bermudez, L. E. & Young, L. S. (1994). Factors affecting invasion of HT-29 and HEp-2 epithelial cells by organisms of the *Mycobacterium avium* complex. *Infect Immun* **62**, 2021–2026.

Bermudez, L. E., Petrofsky, M. & Sangari, F. (2004). Intracellular phenotype of *Mycobacterium avium* enters macrophages primarily by a macropinocytosis-like mechanism and survives in a compartment that differs from that with extracellular phenotype. *Cell Biol Int* **28**, 411–419.

Bermudez, L. E., Petrofsky, M., Sommer, S. & Barletta, R. G. (2010). Peyer's patch-deficient mice demonstrate that *Mycobacterium avium* subsp. *paratuberculosis* translocates across the mucosal barrier via both M cells and enterocytes but has inefficient dissemination. *Infect Immun* **78**, 3570–3577.

Buergelt, C. D., Hall, C., McEntee, K. & Duncan, J. R. (1978). Pathological evaluation of paratuberculosis in naturally infected cattle. *Vet Pathol* **15**, 196–207.

Buza, J. J., Mori, Y., Bari, A. M., Hikono, H., Aodon-geril, Hirayama, S., Shu, Y. & Momotani, E. (2003). *Mycobacterium avium* subsp. *paratuberculosis* infection causes suppression of RANTES, monocyte chemoattractant protein 1, and tumor necrosis factor alpha expression in peripheral blood of experimentally infected cattle. *Infect Immun* **71**, 7223–7227.

Cambier, C. J., Takaki, K. K., Larson, R. P., Hernandez, R. E., Tobin, D. M., Urdahl, K. B., Cosma, C. L. & Ramakrishnan, L. (2014). Mycobacteria manipulate macrophage recruitment through coordinated use of membrane lipids. *Nature* **505**, 218–222.

Cooney, M. A., Steele, J. L., Steinberg, H. & Talaat, A. M. (2014). A murine oral model for *Mycobacterium avium* subsp. *paratuberculosis* infection and immunomodulation with *Lactobacillus casei* ATCC 334. *Front Cell Infect Microbiol* **4**, 11.

David, J., Barkema, H. W., Mortier, R., Ghosh, S., Guan, L. & De Buck, J. (2014). Gene expression profiling and putative biomarkers of calves 3 months after infection with *Mycobacterium avium* subspecies *paratuberculosis*. *Vet Immunol Immunopathol* **160**, 107–117.

Diard, M., Garcia, V., Maier, L., Remus-Emsermann, M. N., Regoes, R. R., Ackermann, M. & Hardt, W. D. (2013). Stabilization of cooperative virulence by the expression of an avirulent phenotype. *Nature* **494**, 353–356.

Early, J. & Bermudez, L. E. (2011). Mimicry of the pathogenic myco-bacterium vacuole *in vitro* elicits the bacterial intracellular phenotype, including early-onset macrophage death. *Infect Immun* **79**, 2412–2422.

Eckstein, T. M., Chandrasekaran, S., Mahapatra, S., McNeil, M. R., Chatterjee, D., Rithner, C. D., Ryan, P. W., Belisle, J. T. & Inamine, J. M. (2006). A major cell wall lipopeptide of *Mycobacterium avium* subspecies *paratuberculosis*. *J Biol Chem* **281**, 5209–5215.

Edgar, R., Domrachev, M. & Lash, A. E. (2002). Gene Expression Omnibus: NCBI gene expression and hybridization array data reposi-tory. *Nucleic Acids Res* **30**, 207–210.

Ehrt, S. & Schnappinger, D. (2007). *Mycobacterium tuberculosis* virulence: lipids inside and out. *Nat Med* **13**, 284–285.

Facciuolo, A., Kelton, D. F. & Mutharia, L. M. (2013). Novel secreted antigens of *Mycobacterium paratuberculosis* as serodiagnostic bio-markers for Johne's disease in cattle. *Clin Vaccine Immunol* **20**, 1783–1791.

Fratti, R. A., Chua, J., Vergne, I. & Deretic, V. (2003). *Mycobacterium tuberculosis* glycosylated phosphatidylinositol causes phagosome maturation arrest. *Proc Natl Acad Sci U S A* **100**, 5437–5442.

Freund, J. (1956). The mode of action of immunologic adjuvants. *Bibl Tuberc* **10**, 130–148.

Geisel, R. E., Sakamoto, K., Russell, D. G. & Rhoades, E. R. (2005). In vivo activity of released cell wall lipids of *Mycobacterium bovis* bacillus Calmette-Guérin is due principally to trehalose mycolates. *J Immunol* **174**, 5007–5015.

Hagblom, P., Segal, E., Billyard, E. & So, M. (1985). Intragenic recom-bination leads to pilus antigenic variation in *Neisseria gonorrhoeae*. *Nature* **315**, 156–158.

Harriff, M. & Bermudez, L. E. (2009). Environmental amoebae and mycobacterial pathogenesis. *Methods Mol Biol* **465**, 433–442.

Hines, M. E., II, Stabel, J. R., Sweeney, R. W., Griffin, F., Talaat, A. M., Bakker, D., Benedictus, G., Davis, W. C., de Lisle, G. W. & other authors (2007). Experimental challenge models for Johne's disease: a review and proposed international guidelines. *Vet Microbiol* **122**, 197–222.

Hines, M. E. II, Turnquist, S. E., Ilha, M. R., Rajeev, S., Jones, A. L., Whittington, L., Bannantine, J. P., Barletta, R. G., Gröhn, Y. T. & other authors (2014). Evaluation of novel oral vaccine candidates and validation of a caprine model of Johne's disease. *Front Cell Infect Microbiol* **4**, 26.

Khan, F. A., Chaudhry, Z. I., Ali, M. I., Khan, S., Mumtaz, N. & Ahmad, I. (2010). Detection of *Mycobacterium avium* subsp. *paratuberculosis* in tissue samples of cattle and buffaloes. *Trop Anim Health Prod* **42**, 633–638.

Khare, S., Lawhon, S. D., Drake, K. L., Nunes, J. E., Figueiredo, J. F., Rossetti, C. A., Gull, T., Everts, R. E., Lewin, H. A. & other authors (2012). Systems biology analysis of gene expression during *in vivo Mycobacterium avium paratuberculosis* enteric colonization reveals role for immune tolerance. *PLoS One* **7**, e42127.

Konnai, S., Usui, T., Ohashi, K. & Onuma, M. (2003). The rapid quantitative analysis of bovine cytokine genes by real-time RT-PCR. *Vet Microbiol* **94**, 283–294.

Lee, H., Stabel, J. R. & Kehrli, M. E., Jr (2001). Cytokine gene expression in ileal tissues of cattle infected with *Mycobacterium paratuberculosis*. *Vet Immunol Immunopathol* **82**, 73–85.

Livak, K. J. & Schmittgen, T. D. (2001). Analysis of relative gene expression data using real-time quantitative PCR and the $2^{-\Delta\Delta C_T}$ method. *Methods* **25**, 402–408.

McNabe, M., Tennant, R., Danelishvili, L., Young, L. & Bermudez, L. E. (2011). *Mycobacterium avium* ssp. *hominissuis* biofilm is composed of distinct phenotypes and influenced by the presence of antimicrobials. *Clin Microbiol Infect* **17**, 697–703.

McNamara, M., Tzeng, S. C., Maier, C., Zhang, L. & Bermudez, L. E. (2012). Surface proteome of "*Mycobacterium avium* subsp. *hominissuis*" during the early stages of macrophage infection. *Infect Immun* **80**, 1868–1880.

Minnikin, D. (1982). Lipids: complex lipids, their chemistry, biosynthesis and roles. In *The Biology of the Mycobacteria*, pp. 95–185. Edited by S. J. Ratledge. London: Academic Press.

Mitchell, R. M., Whitlock, R. H., Stehman, S. M., Benedictus, A., Chapagain, P. P., Grohn, Y. T. & Schukken, Y. H. (2008). Simulation modeling to evaluate the persistence of *Mycobacterium avium* subsp. *paratuberculosis* (MAP) on commercial dairy farms in the United States. *Prev Vet Med* **83**, 360–380.

Mosser, D. M. & Edwards, J. P. (2008). Exploring the full spectrum of macrophage activation. *Nat Rev Immunol* **8**, 958–969.

Ott, S. L., Wells, S. J. & Wagner, B. A. (1999). Herd-level economic losses associated with Johne's disease on US dairy operations. *Prev Vet Med* **40**, 179–192.

Patel, D., Danelishvili, L., Yamazaki, Y., Alonso, M., Paustian, M. L., Bannantine, J. P., Meunier-Goddik, L. & Bermudez, L. E. (2006). The ability of *Mycobacterium avium* subsp. *paratuberculosis* to enter bovine epithelial cells is influenced by preexposure to a hyperosmolar environment and intracellular passage in bovine mammary epithelial cells. *Infect Immun* **74**, 2849–2855.

Penketh, A., Pitt, T., Roberts, D., Hodson, M. E. & Batten, J. C. (1983). The relationship of phenotype changes in *Pseudomonas aeruginosa* to the clinical condition of patients with cystic fibrosis. *Am Rev Respir Dis* **127**, 605–608, .

Periasamy, S., Tripathi, B. N. & Singh, N. (2013). Mechanisms of *Mycobacterium avium* subsp. *paratuberculosis* induced apoptosis and necrosis in bovine macrophages. *Vet Microbiol* **165**, 392–401.

Rainwater, D. L. & Kolattukudy, P. E. (1985). Fatty acid biosynthesis in *Mycobacterium tuberculosis* var. *bovis* bacillus Calmette-Guérin. Purification and characterization of a novel fatty acid synthase, myco-cerosic acid synthase, which elongates n-fatty acyl-CoA with methyl-malonyl-CoA. *J Biol Chem* **260**, 616–623, .

Rocha-Ramírez, L. M., Estrada-García, I., López-Marín, L. M., Segura-Salinas, E., Méndez-Aragón, P., Van Soolingen, D., Torres-González, R., Chacón-Salinas, R., Estrada-Parra, S. & other authors (2008). *Mycobacterium tuberculosis* lipids regulate cytokines, TLR-2/4 and MHC class II expression in human macrophages. *Tuberculosis (Edinb)* **88**, 212–220.

Ryan, G. J., Hoff, D. R., Driver, E. R., Voskuil, M. I., Gonzalez-Juarrero, M., Basaraba, R. J., Crick, D. C., Spencer, J. S. & Lenaerts, A. J. (2010). Multiple *M. tuberculosis* phenotypes in mouse and guinea pig lung tissue revealed by a dual-staining approach. *PLoS One* **5**, e11108.

Sartain, M. J., Dick, D. L., Rithner, C. D., Crick, D. C. & Belisle, J. T. (2011). Lipidomic analyses of *Mycobacterium tuberculosis* based on accurate mass measurements and the novel "Mtb LipidDB". *J Lipid Res* **52**, 861–872.

Scandurra, G. M., de Lisle, G. W., Cavaignac, S. M., Young, M., Kawakami, R. P. & Collins, D. M. (2010). Assessment of live candidate vaccines for paratuberculosis in animal models and macrophages. *Infect Immun* 78, 1383–1389.

Schneider, C. A., Rasband, W. S. & Eliceiri, K. W. (2012). NIH Image to ImageJ: 25 years of image analysis. *Nat Methods* 9, 671–675.

Sigurethardóttir, O. G., Valheim, M. & Press, C. M. (2004). Establishment of *Mycobacterium avium* subsp. *paratuberculosis* infection in the intestine of ruminants. *Adv Drug Deliv Rev* 56, 819–834.

Smythies, L. E., Sellers, M., Clements, R. H., Mosteller-Barnum, M., Meng, G., Benjamin, W. H., Orenstein, J. M. & Smith, P. D. (2005). Human intestinal macrophages display profound inflammatory anergy despite avid phagocytic and bacteriocidal activity. *J Clin Invest* 115, 66–75.

Souza, C., Davis, W. C., Eckstein, T. M., Sreevatsan, S. & Weiss, D. J. (2013). Mannosylated lipoarabinomannans from *Mycobacterium avium* subsp. *paratuberculosis* alters the inflammatory response by bovine macrophages and suppresses killing of *Mycobacterium avium* subsp. *avium* organisms. *PLoS One* 8, e75924.

Stabel, J. R. (1998). Johne's disease: a hidden threat. *J Dairy Sci* 81, 283–288.

Stabel, J. R. & Robbe-Austerman, S. (2011). Early immune markers associated with *Mycobacterium avium* subsp. *paratuberculosis* infection in a neonatal calf model. *Clin Vaccine Immunol* 18, 393–405.

Subramoni, S., Agnoli, K., Eberl, L., Lewenza, S. & Sokol, P. A. (2013). Role of *Burkholderia cenocepacia afcE* and *afcF* genes in determining lipid-metabolism-associated phenotypes. *Microbiology* 159, 603–614.

Sugawara, I., Yamada, H., Kaneko, H., Mizuno, S., Takeda, K. & Akira, S. (1999). Role of interleukin-18 (IL-18) in mycobacterial infection in IL-18-gene-disrupted mice. *Infect Immun* 67, 2585–2589.

Sweeney, R. W., Whitlock, R. H. & Rosenberger, A. E. (1992). *Mycobacterium paratuberculosis* cultured from milk and supramammary lymph nodes of infected asymptomatic cows. *J Clin Microbiol* 30, 166–171.

Tuchscherr, L., Medina, E., Hussain, M., Völker, W., Heitmann, V., Niemann, S., Holzinger, D., Roth, J., Proctor, R. A. & other authors (2011). *Staphylococcus aureus* phenotype switching: an effective bacterial strategy to escape host immune response and establish a chronic infection. *EMBO Mol Med* 3, 129–141.

Weigoldt, M., Meens, J., Doll, K., Fritsch, I., Möbius, P., Goethe, R. & Gerlach, G. F. (2011). Differential proteome analysis of *Mycobacterium avium* subsp. *paratuberculosis* grown *in vitro* and isolated from cases of clinical Johne's disease. *Microbiology* 157, 557–565.

Weiss, D. J., Evanson, O. A., Moritz, A., Deng, M. Q. & Abrahamsen, M. S. (2002). Differential responses of bovine macrophages to *Mycobacterium avium* subsp. *paratuberculosis* and *Mycobacterium avium* subsp. *avium*. *Infect Immun* 70, 5556–5561.

Weiss, D. J., Evanson, O. A. & Souza, C. D. (2006). Mucosal immune response in cattle with subclinical Johne's disease. *Vet Pathol* 43, 127–135.

Whittington, R. J., Marsh, I. B., Saunders, V., Grant, I. R., Juste, R., Sevilla, I. A., Manning, E. J. & Whitlock, R. H. (2011). Culture phenotypes of genomically and geographically diverse *Mycobacterium avium* subsp. *paratuberculosis* isolates from different hosts. *J Clin Microbiol* 49, 1822–1830.

Wren, B. & Dorrell, N. (2002). *Functional Microbial Genomics*. Amsterdam, Boston: Academic Press.

Edited by: R. Manganelli